Journal of Power Sources 195 (2010) 4957–4962

Contents lists available at ScienceDirect

Journal of Power Sources

journal homepage: www.elsevier.com/locate/jpowsour

Understanding the redox shuttle stability of 3,5-di-*tert*-butyl-1,2-dimethoxybenzene for overcharge protection of lithium-ion batteries

Zhengcheng Zhang[a,*], Lu Zhang[a], John A. Schlueter[b], Paul C. Redfern[a], Larry Curtiss[a,b,c], Khalil Amine[a,1]

[a] Chemical Sciences and Engineering Division, Argonne National Laboratory, 9700 South Cass Avenue, Argonne, IL 60439, USA
[b] Materials Science Division, Argonne National Laboratory, 9700 South Cass Avenue, Argonne, IL 60439, USA
[c] Center for Nanoscale Materials, Argonne National Laboratory, 9700 South Cass Avenue, Argonne, IL 60439, USA

ARTICLE INFO

Article history:
Received 14 January 2010
Received in revised form 22 February 2010
Accepted 23 February 2010
Available online 3 March 2010

Keywords:
3,5-Di-*tert*-butyl-1,2-dimethoxybezene
Redox shuttle
Overcharge protection
Lithium-ion batteries

ABSTRACT

3,5-di-*tert*-butyl-1,2-dimethoxybenzene (DBDB) has been synthesized as a new redox shuttle additive for overcharge protection of lithium-ion batteries. DBDB can easily dissolve in carbonate-based electrolytes, which facilitates its practical use in lithium-ion batteries; however, it has poor electrochemical stability compared to 2,5-di-*tert*-butyl-1,4-dimethoxybenzene (DDB). The structures of DBDB and DDB were investigated using X-ray crystallography and density functional calculations. The structures differ in the conformations of the alkoxy bonds probably due to the formation of an intramolecular hydrogen bond in the case of DBDB. We investigated reaction energies for decomposition pathways of neutral DBDB and DDB and their radical cations and found little difference in the reaction energies, although it is clear that kinetically, decomposition of DBDB is more favorable.

1. Introduction

Redox shuttle additives have been proposed for overcharge protection of secondary lithium-ion batteries for decades [1–6]. Generally, the redox shuttle molecule can be reversibly oxidized and reduced at a defined potential slightly higher than the end-of-charge potential of the positive electrode. This mechanism can protect the cell from overcharge by locking the potential of the positive electrode at the oxidation potential of the shuttle molecules. The detailed mechanism is shown in Scheme 1. On the overcharged positive electrode surface, the redox shuttle molecule (S) would be oxidized to its (radical) cation form (S^+), which, via diffusion across the cell electrolyte, would be reduced back to its original or reduced state on the surface of the negative electrode. The reduced form would then diffuse back to the positive electrode to get oxidized again. The "oxidation–diffusion–reduction–diffusion" cycle could be repeated continuously due to the reversible nature of the redox shuttle to shunt the overcharge current. The redox shuttling mechanism at overcharge can be regarded as a controlled internal short and the net result of the shuttling is to convert the overcharge electricity power into heat to avoid the reactions between the electrodes and electrolytes at high voltage.

In the past 20 years, hundreds of compounds have been reported for the purpose of redox shuttles [7,8]. Looking through the timeline and corresponding literatures, one can easily find out that more and more organic structures have been employed in the design of the redox shuttles, e.g. from inorganic halogen redox couples [9–11] to organometallics ferrocene derivatives [3,12–15], and then to conjugated organic compounds [16–21]. However, with a few exceptions, most of the reported redox shuttles cannot meet the requirements for practical battery applications due to either the low redox potentials of the redox shuttles or the poor stability of the oxidized shuttle molecules, which are two major obstacles for finding successful redox shuttle additives. The stability seems even more important because it is not difficult to find molecules bearing desired oxidation potentials (3.9 V for $LiFeO_4$ positive electrodes, and 4.5 V for $LiMn_2O_4$ positive electrodes), but only a few of them give a certain amount of the overcharge shunting time, comprising 10-methylphenothiazine (MPT) [17], 2,2,6,6-tetramethylpiperinyl-oxides (TEMPO) [18], 2,5-di-*tert*-butyl-1,4-dimethoxybenzene (DDB) [16], and 2-(pentafluorophenyl)-tetrafluoro-1,3,2-benzodioxaborole (PFPTFBDB) [21].

As an organic benzene derivative, DDB has shown promising results. Compared to MPT [17] and TEMPO [18], DDB exhibits a much higher oxidation potential, 3.96 V *vs.* Li, and stable cycling (260 cycles) performance under the condition of 100% overcharge

* Corresponding author at: Chemical Sciences and Engineering Division, Argonne National Laboratory, 9700 South Cass Avenue, Building 205, Argonne, IL 60439, USA. Tel.: +1 630 2527868; fax: +1 630 872 4440.
E-mail addresses: zzhang@anl.gov (Z. Zhang), amine@anl.gov (K. Amine).
[1] Tel.: +1 630 252 3838; fax: +1 630 972 4672.

0378-7753/$ – see front matter © 2010 Elsevier B.V. All rights reserved.
doi:10.1016/j.jpowsour.2010.02.075

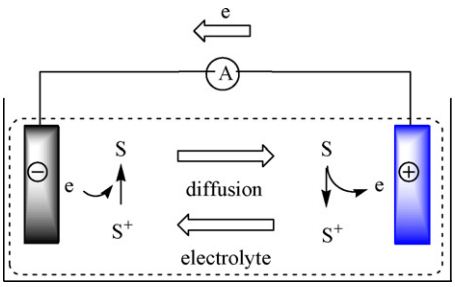

Scheme 1. Scheme of the mechanism of redox shuttle shunting current during overcharge.

in $LiFePO_4$ cells [16]. On the other hand, PFPTFBDB [20] has been reported as having an even higher oxidation potential (4.43 V *vs.* Li/Li^+) and showing promising overcharge results for LiM_xO_2 (M = Ni, Co, Mn, etc.) cells. However, the multiple steps involved in the synthesis of this perfluoro compound make it a great challenge for its scale-up and wide application.

The main impediment to the use of DDB in lithium-ion cells is its low solubility in conventional carbonate electrolytes due to its low polarity [22]. Thus, it is hard to use DDB directly in the conventional electrolyte to achieve the reported experimental results. Also, the factors related to stability of redox shuttles are not fully understood. In this report, we studied DBDB, an isomer of DDB, as a candidate for redox shuttles. The structures and decomposition pathways were compared to those of DDB to explore the possibility of further improvements in their performance.

2. Experimental

DBDB is not commercially available, and it was prepared in our lab according to the following procedure (Fig. 1). First, NaH (1.8 g, 5 equiv.) was added to 3,5-di-*tert*-butylcatechol (2.0 g, 1 equiv., Aldrich) in dry THF (70 mL), and the mixture was stirred under an argon atmosphere. Iodomethane (1.32 mL, 3 equiv., Aldrich) was then added to the reaction mixture through an addition funnel. After 3 h of stirring, the reaction mixture was poured into 100 g ice and neutralized to pH 7 with 10% HCl aqueous solution. The resulting mixture was then extracted with CH_2Cl_2 (3× 20 mL), and the organic phase was concentrated by a rotary evaporator. Finally, the residue was passed through a chromatograph column to generate the pure product (yield 71%). ^1H NMR (500 MHz, $CDCl_3$): δ/ppm 6.93 (s, 1H), 6.83 (s, 1H), 3.87 (s, 6H), 1.39 (s, 9H), 1.31 (s, 9H); ^{13}C NMR (125 MHz, $CDCl_3$): δ/ppm 152.74, 146.37, 145.68, 142.34, 115.92, 108.50, 60.47, 56.04, 35.51, 35.04, 31.81, 30.89. Mass spectroscopy (ESI^+): calcd. (M^+) 250.2, found (M^+) 250.2. Single crystals of DBDB were obtained by storing the concentrated solution at 4 °C and were identified by X-ray crystallography.

Cyclic voltammetry experiments using a Solartron Analytical 1470E system were performed in custom-made three-electrode cells with a 1-mm-diameter Pt working electrode, a Li metal reference electrode, and a Li counter electrode. The electrolyte tested was 1.2 M $LiPF_6$ in a mixture of ethylene carbonate and ethyl methyl carbonate (EC/EMC) in a weight ratio of 3:7. The DBDB shuttle molecule was added to the carbonate in a concentration of 5 wt.%. The sweep rate was varied from 10 to 500 mV s^{-1}. In addition, 1000 successive scans were taken at 100 mV s^{-1}.

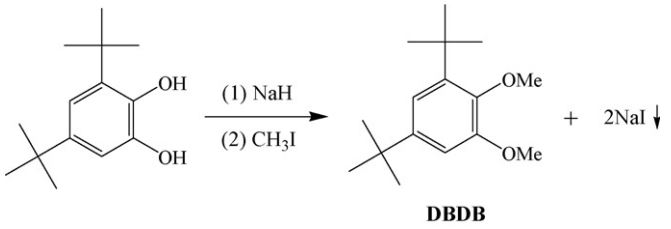

Fig. 1. Synthesis of 3,5-di-*tert*-butyl-1,2-dimethoxybenzene (DBDB).

Overcharge tests were conducted in 2032 coin cells of $LiFePO_4$/Li and $LiFePO_4$/graphite. The graphite electrode consisted of mesocarbon microbeads (MCMB), and the $LiFePO_4$ electrode (provided by EnerDel) consisted of 84% $LiFePO_4$ active material, 8% acetylene carbon black, and 8% polyvinylidene difluoride as binder. The electrolyte was 1.2 M $LiPF_6$ in 3:7 EC/EMC containing 5 wt.% DBDB additive. The cells were charged at a constant current of C/10 for 20 h (100% overcharge) or until a specific upper cutoff voltage was reached (normally 4.5 V *vs.* Li/Li^+), whichever occurred first. After overcharging, the cells were discharged to a normal cutoff voltage using the same constant current.

X-ray diffraction experiments were performed by gluing a single-crystal to the end of a glass fiber and mounted on a Bruker SMART 3-circle diffractometer equipped with an APEX II CCD area detector, sealed-tube MoK_α radiation (λ = 0.71073 Å) X-ray source, graphite monochromator and Monocap collimator. The crystal temperature was maintained at 200 K through use of an Oxford Cryostream 700 Plus cold finger [23].

3. Results and discussion

3.1. Solubility

DBDB is not commercially available, and it was prepared in our lab according to the following procedure (Fig. 1). DBDB shows excellent solubility in carbonate-based electrolyte. The concentration of DBDB in 1.2 M $LiPF_6$ in 3:7 EC/EMC can easily rise to 1.0 mol L^{-1}. According to the principle of "like dissolves like," molecules with large dipole moments will be easily dissolved in the polar carbonate electrolyte. Therefore, the high solubility can be attributed to the large dipole moment of DBDB resulting from its asymmetric structure. Conversely, DDB has a symmetric structure and thus low solubility in polar carbonate-based electrolyte.

3.2. Electrochemical measurements

Fig. 2 shows cyclic voltammograms for 5% DBDB dissolved in 1.2 M $LiPF_6$ in the 3:7 EC/EMC electrolytes with sweep rates of 10, 20, 50, 100, 200, and 500 mV s^{-1}. As shown in Fig. 2a, the DBDB displays a well-defined reversible redox couple. The redox potential of DBDB, evaluated using the mean of the anodic and cathodic potentials [($E_a + E_p$)/2], is 4.20 V *vs.* Li/Li^+, which is 0.24 V higher than that of its DDB counterpart. These results indicate that DBDB could be a suitable redox shuttle for 4-V positive electrodes. After 1000 successive scans using the aforementioned electrolyte at a sweep rate of 100 mV s^{-1}, the redox peaks remained almost unchanged. This result implies the excellent electrochemical reversibility and stability of DBDB.

The diffusion coefficient is another parameter used for evaluating redox shuttles. Fig. 2b plots the anodic peak current (I_p) *vs.* the square root of the sweep rates ($v^{1/2}$). The resulting slope was then substituted into the Randles–Sevcik [19] equation to calculate the diffusion coefficient of DBDB in the electrolyte, which yielded 1.63×10^{-6} cm s^{-1}. One can calculate the minimum concentration of the shuttle necessary for a given charge current by substituting the diffusion coefficient value into the following equation:

$$I = \frac{nFDAC}{L} \quad (1)$$

where I is the current at overcharge; F, the Faraday constant; D, the diffusion coefficient for the redox shuttle; A, electrode area; C, total concentration of the redox shuttle; and L, interelectrode spac-

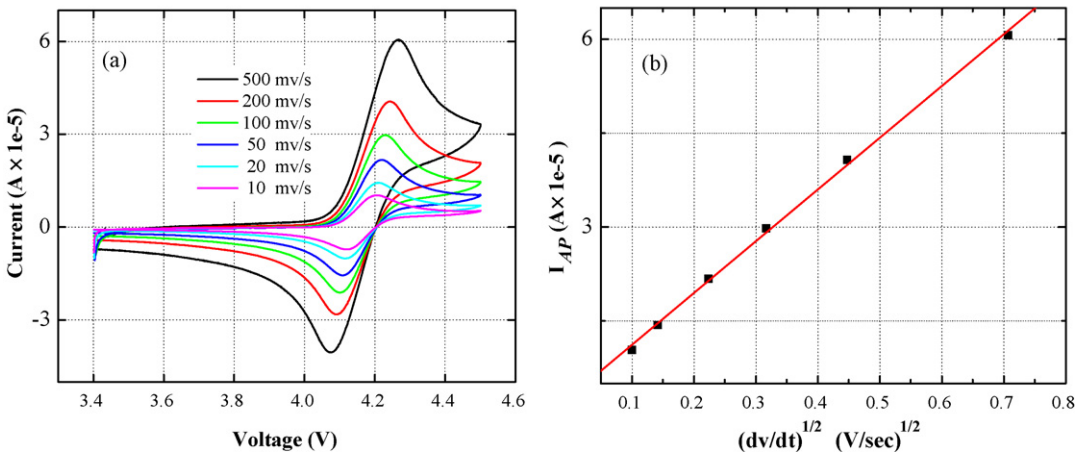

Fig. 2. (a) Cyclic voltammograms of DBDB (0.01 M) in 1.2 M $LiPF_6$ in EC/EMC (3:7 by weight) using a Pt/Li/Li cell at different sweep rates. (b) Plot of I_p vs. $\nu^{1/2}$ used for determination of diffusion constant.

ing. For 18650-type lithium-ion cells, the electrode area could be as low as 650 cm^2, and the interelectrode spacing is 25 μm. When the charge rate is 1C, the current is 3 A, and the DBDB concentration is calculated to be 0.075 M. Given that the shuttle molecule diffusion is slow in the porous separator and electrodes, and the effective diffusion coefficient is about one-third that measured in liquid electrolyte, the minimum DBDB concentration for 1C charge is no less than 0.22 M. This requirement can be easily met since the DBDB concentration can be raised to 1.0 M in the carbonate-based electrolyte.

To explore the overcharge capability of DBDB, overcharge tests were conducted with 2032 coin cells. Fig. 3 shows the overcharge voltage profiles of Li/$LiFeO_4$ cells (top) and MCMB/$LiFeO_4$ cells (bottom) containing 5 wt.% DBDB in 1.2 M $LiPF_6$ in the 3:7 EC/EMC electrolyte. Formation processes were conducted before overcharging test and the initial capacity losses or Coulombic efficiencies of the test cells are identical to those of the control cells containing no redox shuttle additives. During charging of the MCMB/$LiFeO_4$ cells, the lithium-ion was removed from the $LiFePO_4$ positive electrode and intercalated into the MCMB negative electrode. The normal charge took place at about 3.4 V. After the full capacity was attained, the cell voltage rose quickly until it reached 4.05 V, where the redox shuttle mechanism was activated, and the overcharge current was shunted by DBDB molecules.

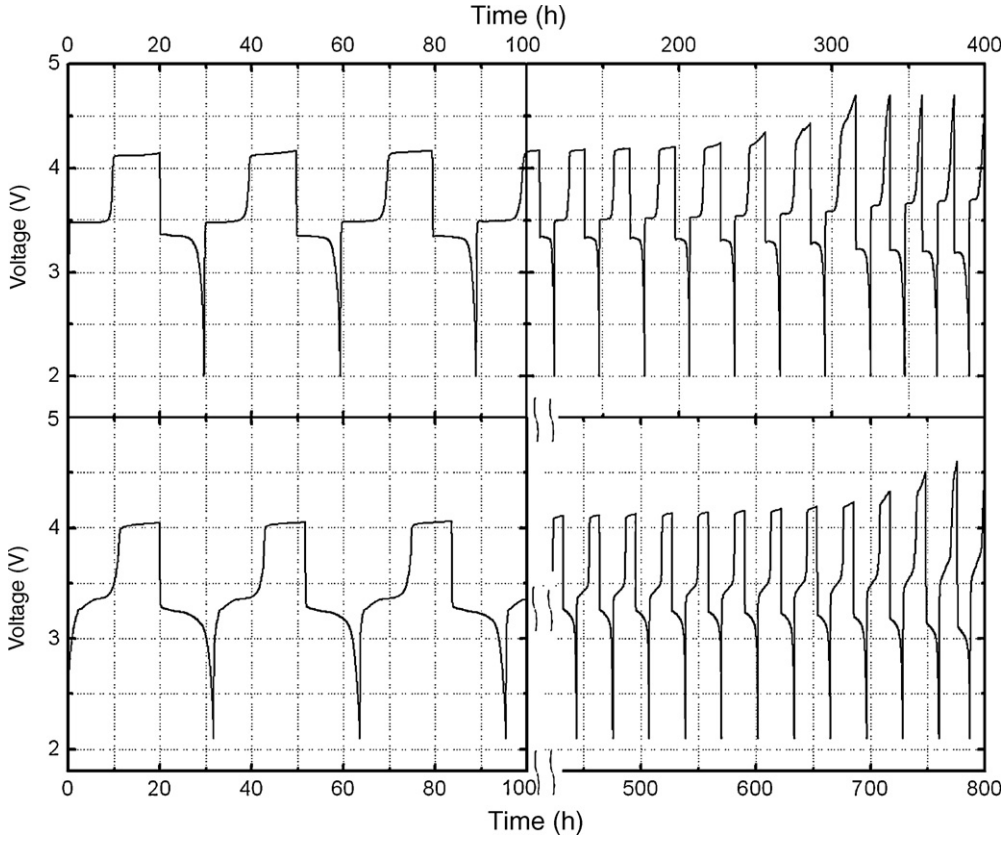

Fig. 3. Voltage profiles of Li/$LiFeO_4$ cell (above) and MCMB/$LiFeO_4$ cell (bottom) containing 5 wt.% DBDB in 1.2 M $LiPF_6$ in EC/EMC (3:7 by weight) during the course of 0–100 h and 100–400 h.

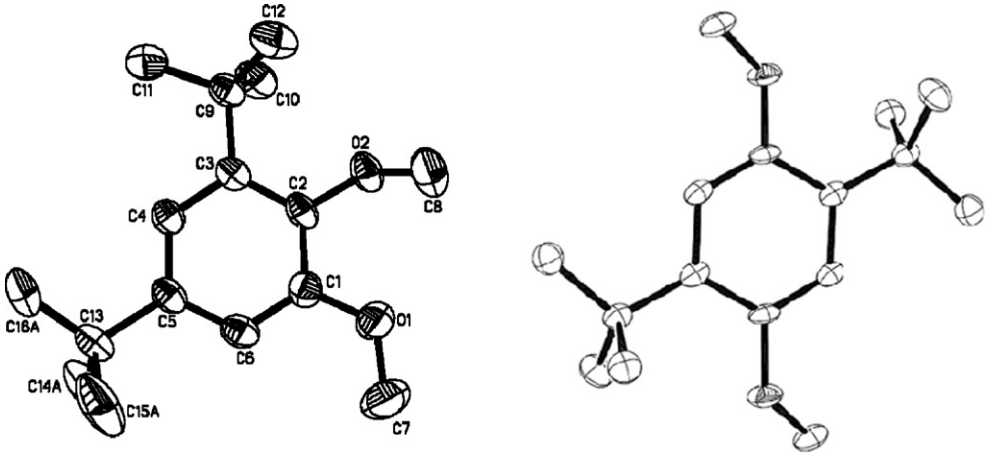

Fig. 4. ORTEP diagram (50% probability ellipsoids) of DBDB (left) and DDB (right).

Table 1
Selected bond distances (in Å) of DBDB and DDB from X-ray crystallography and B3LYP/6-31G* calculations on neutral molecules and radical cations.

DBDB				DDB		
Bond[a]	Crystal structure	B3LYP/6-31G* neutral	B3LYP/6-31G* cation	Bond	B3LYP/6-31G* neutral	B3LYP/6-31G* cation
C1–O1	1.373(4)	1.380	1.315	C (ring)–O	1.375	1.324
C7–O1	1.412(4)	1.417	1.442			
C2–O2	1.391(3)	1.371	1.335	$C(CH_3)$–O	1.414	1.444
C8–O2	1.439(4)	1.430	1.452			

[a] See Fig. 4 for numbering.

The effectiveness of the shuttle molecules was not sustained with cycling. Fig. 3 (top) shows that in Li/$LiFeO_4$ cells, the DBDB could only support 11 cycles at 100% overcharge condition before the shuttle molecule became ineffective. The MCMB/$LiFeO_4$ cells had better though still poor performance, with 20 efficient overcharge cycles, as shown in Fig. 3 (bottom). The results from cycling cells indicate that under the same test condition DBDB is not as stable as DDB, which can survive at least 200 cycles [16].

3.3. Molecular structures and degradation analysis

Even though DBDB and DDB share the same formula, the electrochemical stability of DBDB is much different from that of DDB. To investigate the difference, their molecular structures were investigated by X-ray crystallography and theoretical computation. The single-crystal structures of DBDB and DDB are shown in Fig. 4. As clearly indicated in Fig. 4, the DBDB structure has the two methoxy groups (CH_3O) in different orientations. The methoxy group at C(1) is almost in the plane of the benzene ring pointing to C(6). The dihedral angle between CH_3(7)–O(1) and benzene ring is −10.9° This conformation not only facilitates the conjugation effect between the O(1) and the π electron from the benzene ring due to the vertical orientation of the O(1) *p* orbital, but also helps the *tert*-butyl group at C(5) provide good steric protection to C(6). However, the other methoxy group at C(2) points out of the ring with the dihedral angle between CH_3(8)–O(2) and benzene ring being 119.2°. Based on density functional calculations (see below) we believe that this is due to the formation of an intramolecular hydrogen bond between a C–H bond of the methyl group and the oxygen of the methoxy group attached to C(1). Therefore the conjugation effect between O(2) and the aromatic ring is reduced. This assumption is confirmed by the longer bond distances for C(2)–O(2) or C(8)–O(2) than those of C(1)–O(1) or C(7)–O(1), as summarized in Table 1. However, for the crystal structure of DDB, both methoxy groups are relatively close to the plane of benzene ring and the dihedral angles are 35.2° because there is no intramolecular hydrogen bond possible in DDB. This kind of conformation is favorable for the conjugation of both methoxy groups to the benzene electrons compared to the methoxy group at C(2) of DBDB. The chemical bond distances of CH_3–O and O–C(*sp*2) of DDB are shorter than C(1)–O(1) and C(7)–O(1) of DBDB, respectively.

Fig. 5 shows the optimized structures of the DBDB and DDB neutral molecules and their cation radicals calculated by the B3LYP/6-31G* density functional method [24,25]. The optimized distances of selected bonds in neutral DBDB and DDB molecules are

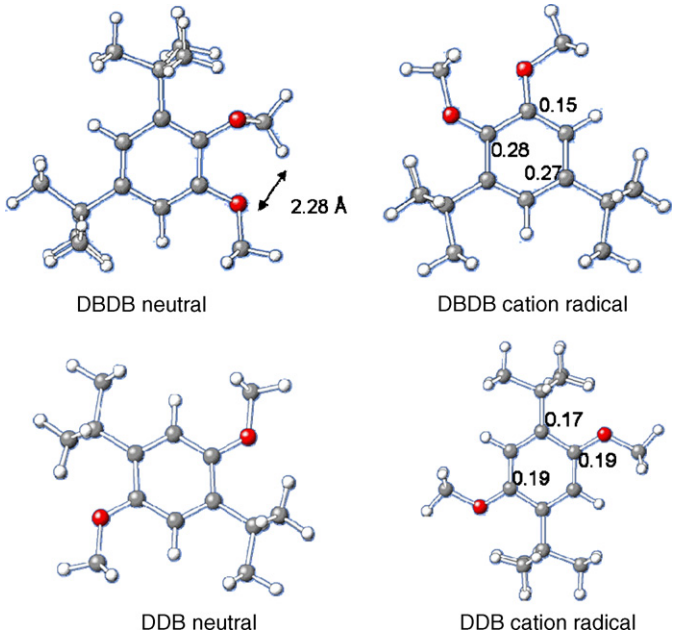

Fig. 5. Optimized structures of DBDB and DDB neutral and cation calculated by the B3LYP/6-31G* method. Spin densities on the cations are shown on selected atoms.

Table 2
Reaction energies (in eV) for various possible decompositions of DBDB and DDB.

Reaction	ΔE_e[a]	ΔG (s, 298 K)[b]	ΔG (s, 298 K)[c]
C–O bond breaking in DBDB			
Neutral: $((CH_3)_3C)_2(CH_3O)_2C_6H_2 \rightarrow ((CH_3)_3C)_2(CH_3O)(O)C_6H_2$[d] $+ CH_3$	2.27	1.35	1.32
Cation+ :$((CH_3)_3C)_2(CH_3O)_2C_6H_2^+ \rightarrow ((CH_3)_3C)_2(CH_3O)(O)C_6H_2^+$[d] $+ CH_3$	2.26	1.37	1.31
C–O bond breaking in DDB			
Neutral: $((CH_3)_3C)_2(CH_3O)_2C_6H_2 \rightarrow ((CH_3)_3C)_2(CH_3O)(O)C_6H_2$[e] $+ CH_3$	2.01	1.17	1.16
Cation: $((CH_3)_3C)_2(CH_3O)_2C_6H_2^+ \rightarrow ((CH_3)_3C)_2(CH_3O)(O)C_6H_2^+$[e] $+ CH_3$	2.48	1.51	1.47
DBDB decomposition to methane			
Neutral: $((CH_3)_3C)_2(CH_3O)_2C_6H_2 \rightarrow ((CH_3)_3C)_2(OCH_2O)C_6H_2$[f] $+ CH_4$	−0.42	−0.94	−0.96
Cation: $((CH_3)_3C)_2(CH_3O)_2C_6H_2^+ \rightarrow ((CH_3)_3C)_2(OCH_2O)C_6H_2^+$[f] $+ CH_4$	−0.21	−0.90	−0.96
DBDB and DDB cation decomposition to ethylene			
DDB+: $((CH_3)_3C)_2(CH_3O)_2C_6H_2 \rightarrow ((CH_3)_3C)_2(OH)_2C_6H_2^+ + C_2H_4$	0.14	−0.82	−1.16
DBDB+: $((CH_3)_3C)_2(CH_3O)_2C_6H_2^+ \rightarrow ((CH_3)_3C)_2(OH)_2C_6H_2^+$[g] $+ C_2H_4$	0.46	−0.83	−1.18

[a] Reaction energy (difference in electronic energies) from a B3LYP/6-31 + G*//B3LYP/6-31G* calculation.
[b] Free energy of reaction at 298 K including solvation energies from a B3LYP/631 + G*//B3LYP/6-31G* calculation. Solvation effects included, via the PCM model with a dielectric constant of 55.
[c] Same as footnote b except the energy is calculated with a larger basis set, B3LYP/6-311 + G(3df,2p).
[d] Structure illustrated by DBDB(–CH_3) in Fig. 5.
[e] Structure illustrated by DBB(–CH_3) in Fig. 5.
[f] Structure illustrated by DBDB(–CH_4) in Fig. 5.
[g] Structure illustrated by DBDB(–C_2H_4) in Fig. 5.

compiled in Table 1, along with the corresponding ones for the radical cations. The calculated structure of the molecule DBDB agrees well with the single-crystal structure even though the surrounding crystal structure is not taken into account in the calculation. The methoxy group at C(2) is pointing out of the aromatic ring, while the other methoxy group at C(1) is in the plane of the benzene ring. There is a short H–O distance (2.28 Å) between the two methoxy groups, which is indicative of the formation of an intramolecular hydrogen bond. For the DDB molecule, both methoxy groups are in the plane of the benzene ring, pointing to the neighboring unsubstituted carbon atom; therefore, the two oxygen atoms are more conjugated with the π electrons.

It is well known that the stability of a redox shuttle depends on decomposition pathways of its oxidized state. The benzene derivative redox shuttles studied here have two possible routes of decomposition during overcharge: the polymerization of the benzene ring and the cleavage of the alkoxy bond. For DDB, polymerization of the benzene ring is believed to be difficult due to the steric hindrance of the two *tert*-butyl groups. We have calculated reaction energies for various decomposition pathways to determine whether this leads to any trends that can explain the stability of DDB over DBDB. We first investigated the energies for breaking the C–O bonds in both the neutrals and cations. The bond energies were calculated using the B3LYP density functional method with the 6-31 + G* and 6-311 + G(3df,2p) basis sets at B3LYP/6-31G* geometries. These methods should give a reasonably accurate account of the reaction energies [26–28]. The results of the B3LYP calculations are given in Table 2. The C–O bond energy in the methoxy bond is slightly larger in neutral DBDB (2.27 eV) than in neutral DDB (2.01 eV). This is probably due in part to the presence of the intramolecular hydrogen bond in DBDB, which stabilizes it relative to DDB. In contrast, breaking the methoxy bond is somewhat easier in the oxidized state of DBDB (2.26 eV) than in the oxidized state of DDB (2.46 eV). In the DBDB cation there is no intramolecular bond formed. Since these C–O bond breaking reactions are endothermic they are unlikely to occur in the electrolytes, but they provide some insight into the strengths of the bonds in the two shuttle molecules.

We also considered decomposition reaction involving methane or ethylene elimination from DDB and DBDB. Both reactions require hydrogen transfer to form the products (see Fig. 6). The decomposition reaction energies were calculated using the same theoretical methods as for the C–O bond energies. The B3LYP results in Table 2 indicate that in this case, the decomposition of DBDB is exothermic by about 1 eV for either the neutral or the cation. The reaction energies for DBB are similar, but the reactions are not likely to occur because of the large distance between the methoxy groups making the hydrogen transfer unlikely. This suggests that the decomposition of the radical cation of DBDB is more likely than for the DBB radical cation. Decomposition of the neutral DBDB is unlikely to occur as oxidation involving electron transfer is a much faster process. Also the spin densities given in Fig. 5 indicate that they are larger for the DBDB radical cation than the DBB cation, which would suggest that former might be more susceptible to polymerization.

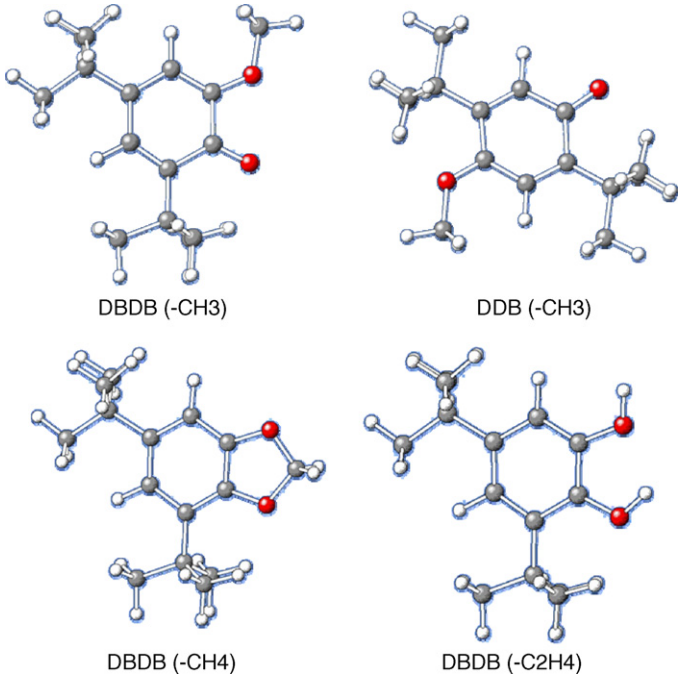

Fig. 6. Structures of decomposition products in Table 2.

4. Conclusions

DBDB was studied as compared to DDB for the purpose of redox shuttle additives for lithium-ion batteries. DBDB shows excellent

solubility in the carbonate-based electrolyte due to its asymmetric structure and larger dipole moment. The structures of the two isomers were investigated using X-ray crystallography and density functional theory. The structures of the DBDB and DDB neutral molecules differ in the conformations of the alkoxy bonds due to the formation of an intramolecular bond in the latter case. We investigated likely decomposition pathways for neutral DBDB and DDB and their radical cations and found reaction pathways that were exothermic. It is clear that kinetically, decomposition of DBDB is more favorable and can explain the poorer stability of DBDB compared to DDB.

Acknowledgements

This research is supported by U.S. Department of Energy, FreedomCAR and Vehicle Technologies Office. Argonne National Laboratory is operated for the U.S. Department of Energy by UChicago Argonne, LLC, under contract DE-AC0Z-06CH11357. The authors thank Dr. Zonghai Chen for the helpful discussions.

References

[1] K.M. Abraham, D.M. Pasquariello, E.B. Willstaedt, J. Electrochem. Soc. 137 (1990) 1856–1857.
[2] M. Jonsson, J. Lind, T. Reitberger, T.E. Eriksen, J. Phys. Chem. 97 (1993) 11278–11282.
[3] M.N. Golovin, D.P. Wilkinson, J.T. Dudley, D. Holonko, S. Woo, J. Electrochem. Soc. 139 (1992) 5–10.
[4] T.J. Richardson, P.N. Ross, J. Electrochem. Soc. 143 (1996) 3992–3996.
[5] M. Adachi, K. Tanaka, K. Sekai, J. Electrochem. Soc. 146 (1999) 1256–1261.
[6] T.J. Richardson, P.N. Ross, Redox shuttle additives for overcharge protection in lithium batteries, in: M.K. Carpenter, D.A. Corrigan (Eds.), Electrochemical Society Proceedings Series, Pennington, NJ, vols. 99–25, 2000, p. 687.
[7] K. Xu, Chem. Rev. 104 (2004) 4303–4417.
[8] Z. Chen, Y. Qin, K. Amine, Electrochim. Acta. 54 (2009) 5605–5613.
[9] W.K. Behl, D.T. Chin, J. Electrochem. Soc. 135 (1988) 16–21.
[10] W.K. Behl, D.T. Chin, J. Electrochem. Soc. 135 (1988) 21–25.
[11] W.K. Behl, J. Electrochem. Soc. 136 (1989) 2305–2310.
[12] K.M. Abraham, M. Needham, D.M. Pasquariello, R.I. Pawtucket, US Patent 4,857,423 (1989).
[13] K.M. Abraham, D.M. Pasquariello, European Patent 0319182 (1989); Canadian Patent 1,244,669 (1989).
[14] S.R. Narayanan, S. Surampudi, A.I. Attia, C.P. Bankston, J. Electrochem. Soc. 138 (8) (1991) 2224–2229.
[15] C.O. Laoire, E. Plichta, M. Hendrickson, S. Mukerjee, K.M. Abraham, Electrochim. Acta. 54 (2009) 6560–6564.
[16] C. Buhrmester, J. Chen, J. Jiang, R.L. Wang, J.R. Dahn, J. Electrochem. Soc. 152 (2005) A2390–A2399.
[17] C. Buhrmester, L. Moshurchak, R.L. Wang, J.R. Dahn, J. Electrochem. Soc. 153 (2006) A288–A294.
[18] C. Buhrmester, L.M. Moshurchak, R.L. Wang, J.R. Dahn, J. Electrochem. Soc. 153 (2006) A1800–A1804.
[19] J.K. Feng, X.P. Ai, Y.L. Cao, H.X. Yang, Electrochem. Commun. 9 (2007) 25–30.
[20] Z. Chen, K. Amine, Electrochem. Commun. 9 (2007) 703–707.
[21] L.M. Moshurchak, W.M. Lamanna, M. Bulinski, R.L. Wang, R.R. Garsuch, J. Jiang, D. Magnuson, M. Triemert, J.R. Dahn, J. Electrochem. Soc. 156 (4) (2009) A309–A312.
[22] J.R. Dahn, J. Jiang, M.D. Fleischauer, C. Buhrmester, L.J. Krause, J. Electrochem. Soc. 152 (2005) A1283–A1289.
[23] Crystal data: C16H26O2, $M = 250.37\,g\,mol^{-1}$, monoclinic, $a = 5.9161(5)$, $b = 28.729(2)$, $c = 9.3759(7)$ Å, $\beta = 98.688(4)^{\circ}$, $V = 1575.3(2)$ Å^3, $T = 200$ K, space group P21/c (no. 14), $Z = 4$, ρcalcd = 1.056 $Mg\,m^{-3}$, μ(Mo-Kα) = 0.067 mm^{-1}, 8672 reflections measured, 1643 unique (Rint = 0.0369) which were used in all calculations. The final wR(F2) was 0.1386, final $R_1 = 0.0476$ for 1248 with $I > 2\sigma(I)$. CCDC nnnnnn contains the supplementary crystallographic data for this paper. These data can be obtained free of charge from The Cambridge Crystallographic Data Centre via www.ccdc.cam.ac.uk/data_request/cif.
[24] M.J. Frisch, G.W. Trucks, H.B. Schlegel, G.E. Scuseria, M.A. Robb, J.R. Cheeseman, J.A. Montgomery Jr., T. Vreven, K.N. Kudin, J.C. Burant, J.M. Millam, S.S. Iyengar, J. Tomasi, V. Barone, B. Mennucci, M. Cossi, G. Scalmani, N. Rega, G.A. Petersson, H. Nakatsuji, M. Hada, M. Ehara, K. Toyota, R. Fukuda, J. Hasegawa, M. Ishida, T. Nakajima, Y. Honda, O. Kitao, H. Nakai, M. Klene, X. Li, J.E. Knox, H.P. Hratchian, J.B. Cross, V. Bakken, C. Adamo, J. Jaramillo, R. Gomperts, R.E. Stratmann, O. Yazyev, A.J. Austin, R. Cammi, C. Pomelli, J.W. Ochterski, P.Y. Ayala, K. Morokuma, G.A. Voth, P. Salvador, J.J. Dannenberg, V.G. Zakrzewski, S. Dapprich, A.D. Daniels, M.C. Strain, O. Farkas, D.K. Malick, A.D. Rabuck, K. Raghavachari, J.B. Foresman, J.V. Ortiz, Q. Cui, A.G. Baboul, S. Clifford, J. Cioslowski, B.B. Stefanov, G. Liu, A. Liashenko, P. Piskorz, I. Komaromi, R.L. Martin, D.J. Fox, T. Keith, M.A. Al-Laham, C.Y. Peng, A. Nanayakkara, M. Challacombe, P.M.W. Gill, B. Johnson, W. Chen, M.W. Wong, C. Gonzalez, J.A. Pople, Gaussian 03 Revision C. 02, Gaussian, Inc., Wallingford CT, 2004.
[25] A.D. Becke, J. Chem. Phys. 98 (1993) 5648–5652.
[26] L.A. Curtiss, K. Raghavachari, P.C. Redfern, J.A. Pople, J. Chem. Phys. 106 (1997) 1063–1079.
[27] L.A. Curtiss, P.C. Redfern, K. Raghavachari, J.A. Pople, J. Chem. Phys. 109 (1998) 42–55.
[28] L.A. Curtiss, P.C. Redfern, K. Raghavachari, J. Chem. Phys. 123 (2005), pp. 124107-124107-12.